X-682-76-149
PREPRINT

SURFACE CHEMISTRY OF SELECTED LUNAR REGIONS

MICHAEL J. BIELEFELD
ROBERT C. REEDY
ARNOLD E. METZGER
JACOB I. TROMBKA
JAMES R. ARNOLD

JUNE 1976

GSFC
GODDARD SPACE FLIGHT CENTER
GREENBELT, MARYLAND

Surface Chemistry of Selected Lunar Regions

Michael J. Bielefeld
Computer Sciences Corporation
Silver Springs, Maryland

Robert C. Reedy
Los Alamos Scientific Lab.
Los Alamos, New Mexico

Albert E. Metzger
Jet Propulsion Lab.
Pasadena, California

J. I. Trombka
Goddard Space Flight Center
Greenbelt, Maryland

and

James R. Arnold
Univ. of Calif. San Diego
La Jolla, California

Abstract

A completely new analysis has been carried out on the data from the Apollo 15 and 16 gamma ray spectrometer experiments. The components of the continuum background have been estimated. The elements Th, K, Fe and Mg give useful results; results for Ti are significant only for a few high Ti regions. Errors are given, and the results are checked by other methods. Concentrations are reported for about sixty lunar regions; the ground track has been subdivided in various ways. The borders of the maria seem well-defined chemically, while the distribution of KREEP is broad. This wide distribution requires emplacement of KREEP before the era of mare formation. Its high concentration in western mare soils seems to require major vertical mixing.

Surface Chemistry of Selected Lunar Regions

Michael J. Bielefeld
Computer Sciences Corporation
Silver Springs, Maryland

Robert C. Reedy
Los Alamos Scientific Lab.
Los Alamos, New Mexico

Albert E. Metzger
Jet Propulsion Lab.
Pasadena, California

J. I. Trombka
Goddard Space Flight Center
Greenbelt, Maryland

and

James R. Arnold
Univ. of Calif. San Diego
La Jolla, California

Abstract

A completely new analysis has been carried out on the data from the Apollo 15 and 16 gamma ray spectrometer experiments. The components of the continuum background have been estimated. The elements Th, K, Fe and Mg give useful results; results for Ti are significant only for a few high Ti regions. Errors are given, and the results are checked by other methods. Concentrations are reported for about sixty lunar regions; the ground track has been subdivided in various ways. The borders of the maria seem well-defined chemically, while the distribution of KREEP is broad. This wide distribution requires emplacement of KREEP before the era of mare formation. Its high concentration in western mare soils seems to require major vertical mixing.

Introduction

A gamma ray spectrometer experiment was carried on the CSM on Apollo 15 and 16, to map the content of the radioactive elements and of some major elements in the surface layers of the lunar regolith. The experimental arrangement has been described by Harrington et al (1974); the basic theory is set forth in Reedy et al (1973) (hereafter called RAT).

The results of mapping for total radioactivity on a 2^{o} grid --- in effect for thorium, which contributes most of the counts on the moon --- may be seen in Frontispiece (1973); more specialized results appear in other publications (Trombka et al, 1973; Metzger et al, 1973; Reedy et al, 1975).

The production of a final analysis of the data is complicated by the fact that we are dealing with a complex spectrum of lines, many of which overlap and blend, seen against a continuum whose shape is not exactly known a priori, and which contributes most of the intensity. The results reported here represent a complete re-analysis of all aspects of the data, taking advantage of new information on the continuum and the basic nuclear processes and including some blocks of data not previously used. The resulting improvements have made possible the application of independent checks, and the calculation of errors.

In this analysis the data have been broken down by region in a number of different ways guided by our general knowledge of lunar history and geography. We report here results for about sixty such regions. The implications of the new results for the development of lunar surface chemistry, and for some local problems, are considered in the discussion.

Analytical Section

Data Selection Criteria

The data used in this analysis comprised approximately 60% of the total lunar Apollo gamma ray data base. The criteria for inclusion were that there be no parity or telemetry errors and that the boom be fully extended to 7.6 meters and be oriented toward the moon to within 30° of the normal to the lunar surface. Care was also taken to avoid data collected immediately after a prolonged boom retraction, which contaminated the lunar data by an increase in the induced neutron activation of the NaI crystal. Data before LM separation and orbital circularization was also excluded.

Adjustment for Gain, Zero, Altitude, Live Time

The Apollo 15 instrument showed a considerable monotonic drift in energy gain with time, and an overall zero drift of some tenths of a channel. The Apollo 16 instrument had no measureable zero drift and a total gain drift of about 8%. Data have been corrected for gain and zero using the position of the positron peak and other peaks as a function of time. Altitude variation during the mission was corrected for, assuming count rates varying as the solid angle subtended by the moon, to a mean altitude of 110 km. A measured instrument live time correction (average about 75%) was also applied.

Background Corrections

The process of extracting the net spectrum due to discrete lunar gamma ray lines, which contains all of the chemical information, from the total measured spectrum is graphically presented in Fig. 1. The total intensities of several of the background components are larger than or comparable to that of the desired line spectrum. The analysis of the background depends on the analysis of the astrophysical gamma ray measurements made away from the moon during the return flight to earth. A re-analysis of this data

has recently been completed (Trombka et al, 1976a). A summary of the contributions to the average Apollo 16 lunar spectrum is presented in Table 1. This and other steps of the analysis have been carried out independently for the two missions. Much has been learned from the comparisons.

Spacecraft Activation Background

The same processes which activate the lunar surface are also activating the lunar orbiting module. The best estimate of the contribution to the total measured spectrum comes from comparison of the measured spectra at two boom lengths during the lunar phase of the Apollo 16 mission. During the trans-earth coast (TEC) portion of the mission spectra were taken at four boom lengths. A comparison of the lunar and TEC results shows that the portion of the spectrum due to spacecraft activation, as measured at the nominal extension of 7.6 meters, was up by a factor of two during the lunar phase. The lunar neutron albedo is the presumed cause of this increase. The model used to derive this contribution includes average spacecraft size, density, relative position with multiple scattering and absorption of internally generated photons.

Electron Bremsstrahlung

The contribution of electron bremsstrahlung to the total measured spectrum was first noticed when a comparison of the trans-earth coast spectra showed the Apollo 16 total intensity to be 15% higher than the Apollo 15 intensity. The only satisfactory explanation of both intensity and spectral shape is electron bremsstrahlung in the local mass around the detector. The IMP-5 detector showed a factor of two increase in the integral flux of 3-12 MeV electrons between the two missions (M. Van Hollebeke, priv. comm.). The smoothed spectrum of this component for

Apollo 16 assuming an isotropic flux of electrons is included in Figure 1.

Primary Proton and Secondary Neutron Induced Activity in the Detector

One of the more difficult background corrections is the radioactivity induced in the detector itself by both primary protons and secondary neutrons. As a result of passive activation experiments on Apollo 17 (Dyer, et al, 1975) and the Apollo-Soyuz Test Project (Trombka et al, 1976b) and a semi-empirical computer simulation by Dyer et al (1975), estimates of the detector activation for the Apollo 15 and 16 missions have been provided by C. S. Dyer (priv. comm.). These estimates, given in Table 1 and depicted in Figure 1, include activation by doses of trapped protons, cosmic proton fluxes, and the lunar neutron albedo.

Lunar Continuum Background

The strongest background component, accounting for over half of all radiation recorded by the Apollo detectors, comes from the continuum developed in the topmost material of the lunar surface. This continuum includes Compton scattered photons, electron bremsstrahlung, and other minor components. The shape and intensity were obtained as follows. The total average lunar gamma ray spectrum for each mission was corrected for all the above sources of background. A best ground truth estimate of the average chemistry was made (see below) and the calculated line spectrum response function subtracted also. The net count rate spectrum due to the lunar continuum was smoothed using a cubic spline program. The result is shown as the multiple scatter component in Figure 1. It shows an $E^{-1.5}$ shape over broad areas, but is flatter in the 4-7 MeV region. Essentially the same shape was derived from the Apollo 15 and 16 data. However, an intensity increase of 5% was needed for Apollo 16, apparently because of a 3% increase of the primary proton flux above that of the Apollo 15 mission.

Continuum Background Due to Variation in Lunar Natural Radioactivity

On each mission only a small variation was observed over the ground track in the total count rate above 2.75 MeV, while large changes were seen in count rate between 0.55 and 2.75 MeV, reflecting differences in concentration of Th, K, and U. Photons from these elements, which are Compton scattered in the lunar surface, contribute a steeply falling continuum in this region. This count-rate-dependent continuum was determined by comparison to a base region containing very low concentrations of the radioactive elements. The highland material of the western crossover region served as the standard on both missions. This part of the lunar continuum was found to be fit best by an exponential function of the energy (E) of the form A exp $(-bE)$ where b is a constant and A is a linear function of the integral count rate for $0.55 \leq E < 2.75$ MeV.

Other Backgrounds

The material in the immediate vicinity of the detector is activated and produces line structure which shows no boom length dependence. The spectrum of lines produced in the local mass shown in Figure 1 was isolated from the trans-earth coast data and probably is modified by the increased neutron flux near the moon. However, little hope exists for improving this first estimate by isolating this component directly from the lunar spectrum, since the local mass lines and discrete lunar lines are measured simultaneously. The amount of radiation in this spectrum and the cosmic diffuse gamma ray background corrected for solid angle of the occulting moon are given in Table 1 and are dealt with in more detail by Trombka et al (1976a).

Elemental Response Functions

In order to unfold the chemical information contained in the measured pulse height spectra, two transformation processes are needed. The first transformation specifies the energy deposition of a monoenergetic photon

in a 7 cm x 7 cm NaI crystal and is described by Berger and Seltzer (1972). In our analysis no error was directly attributed to these Monte Carlo response functions or to the weighted average mass attenuation by the mantle around the detector crystal which was determined to be 6.0 grams/cm^2 of aluminum (Parker, 1975) because the uncertainties of these factors were significantly less than other sources of error. The resolutions of the Apollo 15 and 16 detectors were 8.8% and 7.4% respectively, at the Cs-137 line and varied as $E^{-1/3}$. The construction of the response functions included the non-linearity of the NaI crystal in the 0.2 to 2.5 MeV region proposed by Heath et al (1965).

The second data set needed connects an elemental composition on the lunar surface to a photon flux from natural radioactivity or cosmic ray activation. The basis for this transformation is described by Reedy and Arnold (1972) and details of its application by Reedy et al (1973) (RAT).

Basic Nuclear Data

A new library of gamma ray line source strengths was used for this analysis. Some of the gamma ray line fluxes reported in RAT have been revised using recent more accurate data, and the fluxes for many additional lines have been calculated. The models and procedures used to calculate the fluxes are the same as those described in RAT. The gamma ray fluxes from minor and trace elements were calculated for a range of lunar chemistries and were found to make insignificant contributions to the lunar gamma ray spectra.

The yields for the gamma rays produced by the decay of K, Th, U and their daughters were determined for all lines with yields per parent disintegration greater than 0.005. The fluxes for some of the lines reported in RAT were changed slightly.

The fluxes of the gamma ray lines produced by neutron-capture reactions

were recalculated using new values for yields of a given line per neutron capture and a new set of total neutron-capture rates as a function of depth in the moon. The total neutron-capture rates in the moon for the Apollo 15 and 16 missions were taken from the rates for the $^{10}B(n,\alpha)^{7}Li$ reactions observed during the Apollo 17 mission by the Lunar Neutron Probe Experiment (Woolum et al, 1975). The total neutron capture rates used in calculating the present set of gamma ray line fluxes from neutron-capture reactions were 0.67 of the rates used in RAT.

New cross sections for neutron nonelastic-scattering reactions were evaluated using many new measurements and, together with the same set of particle fluxes used in RAT, were used to calculate gamma ray line intensities from the moon. The largest changes from the nonelastic-scatting fluxes reported in RAT were for the $^{16}O(n,n\alpha\gamma)^{12}C$ reaction (up a factor of 2.64), for the three $^{16}O(n,\alpha\gamma)^{13}C$ reactions (up about 1.25), for the two $^{40}Ca(n,n\gamma)^{40}Ca$ reactions (up about 1.4), and for the $^{48}Ti(n,n\gamma)^{48}Ti$ reaction (up 1.85). The gamma ray lines produced by the decay of radioactivity induced by solar-cosmic-ray (SCR) particles were calculated for each mission using satellite measurements of proton fluxes. Long-term proton fluxes inferred from radioactivities observed in the top layers of rocks were used to calculate the activity profiles and gamma ray line fluxes expected from the decay of SCR-produced ^{56}Co, ^{54}Mn, ^{48}V, ^{26}Al and ^{22}Na at the times of the Apollo 15 and 16 missions.

Gamma ray lines from high-energy nuclear reactions were not considered in PAT. Measurements of the gamma-rays produced by the spallation reactions of high-energy protons with a number of target elements have shown that certain gamma ray lines are strongly produced from each target (cf. Foley et al, 1962). Cross sections for the stronger of the spallation-induced gamma ray lines

were used to calculate the fluxes of these lines from the moon. For typical lunar chemical compositions, the three most intense spallation-induced gamma rays were the 1.634 and 2.613 MeV lines from the de-excitation of ^{20}Ne and the 1.369 MeV line of ^{24}Mg, the important targets for these reactions being magnesium, aluminum, and silicon.

The major elemental response functions are shown in Figure 2.

Ground Truth Normalization

Because of imperfections in the basic nuclear data, and in the RAT model, errors in the absolute determination of non-radioactive elements are to be expected; these are controlled by normalization to one or more ground truth sites.

In the present analysis this was done using several regions each for Apollo 15 and 16. The basic data used were bulk soil analyses at appropriate landing sites. They are given in Table 2. In two cases the results have been adjusted for known admixtures of KREEP (highland composition from Apollo 16, and western mare composition from Apollo 12). Mean chemical compositions for the whole ground tracks were calculated by estimating the fraction of the ground track covered by material of each type. The ground tracks cover more mare material than the lunar average; the trends are consistent with the results of Turkevich (1973). The composition of the Van der Graaff or BBB region (see below) was taken from our own data; this is a small contribution to the total and applies only to Apollo 15.

Finally the matrix inversion results from four or five large representative regions, and for the whole ground track, were separately normalized for Fe, Mg, Ti, and Al, to the chemical values in Table 2. The mean normalization factor for each mission was adopted, and is also shown in Table 2. The errors given are errors of the mean, estimated from the internal scatter of

the normalization factors.

For O and Si, the variation over the lunar surface is smaller than our analytical error, although both elements produce major components of the spectrum. Our procedure was to fix these elements for each mission from the analysis of the whole ground track; the required ground truth factors are of the order of those shown. The value for Ca, which could not be usefully determined, was also fixed at 7% throughout.

For the radioactive elements no such normalization should be or is required. We combined Th and U as a single component, using a factor 3.8 for their ratio. The reported Th values were derived from this component. The values of K in the final Apollo 15 and 16 analyses were systematically low, reflecting some problem with the continuum in the 1.3 MeV region. We have added 300 ppm to the matrix inversion values of K for Apollo 15 and 200 ppm for Apollo 16; a slight lowering of the continuum in this region would accomplish the same result.

Results

The data were accumulated by region, the background subtracted, and the matrix inversion analyses carried out as described in RAT. Ground truth factors were applied for the non-radioactive elements. The results are presented in Tables 4 and 5. The analyses were carried out in one step using the entire data set from channels 40 to 450 (0.75 to 8.8 MeV). This is a more straightforward procedure than that used in Metzger et al (1974); it is made possible by the new work described above. The unstarred regions are defined by longitude boundaries and the coverage of the ground track. The reader will find Frontispiece (1973) useful in defining the areas covered, though it must be kept in mind that coverage is not necessarily uniform. The boundaries of the starred regions are described in the footnotes; the

detailed region boundaries are available from the authors.

Errors

In the elaborate procedure of analysis summarized above, there are numerous sources of error to be considered. The ground truth normalization, while introducing another component of random error, reduces or eliminates most sources of systematic error. To evaluate the random errors in the final results, we have relied mainly on internal consistency. For some purposes a formal error analysis is useful, while the checks discussed below give an independent control.

The hypothesis that certain large blocks of our data sample a chemically homogeneous surface---for example the western backside highlands---is a conservative starting point. The scatter observed when two, four or many sub-regions are analyzed and compared is an upper limit to the true uncertainty in regions of this type, since there may be true variation. As expected from general considerations, this scatter does not depend much on counting time for the best-determined elements, in particular Th. For very short counting times the percentage error begins to rise as $t^{-1/2}$. As we move toward more poorly determined elements, this t-dependent error grows in importance, until for Al only the data for large accumulations are reliable.

The results reported in this paper were somewhat arbitrarily restricted to regions of total accumulation time more than 2000 seconds. For much shorter times, only Th can be measured with useful accuracy. At 2000 seconds the statistical error in Fe and K values is significant, while for Mg it is dominant. The error estimates in Table 3 reflect this.

Errors not due to counting statistics are of two types, absolute and relative. At high concentration, errors due to ground truth normalization

and related problems dominate, and these are proportional to the concentration. At low levels the error of the continuum is most important, and this introduces an absolute uncertainty. In the case of Ti, new nuclear data have reduced the calculated line intensity, and the interference (non-orthogonality) with O is particularly large. Here the "low level" case unfortunately applies in most areas, and an error of 1-1.5% is usual. Our matrix inversion calculations only give useful results in a few high-Ti regions. Other significant interference problems are Si-Al and to a lesser extent Fe-O.

To compute total errors, the two terms in Table 3 should be combined quadratically.

In the case of Fe, there is another source of error not yet controlled, due to modifications in the neutron spectrum in regions of high total capture cross section. This makes the Fe values in KREEP-rich regions systematically low, perhaps by as much as 25-30%.

Checks

There are at least three other ways to analyze the data, which provide checks for the results reported. For Th especially, direct peak fitting of the 2.61 MeV line is possible. The agreement is good.

A second method is to select an energy band in which one element has the greatest effect on variations in the total count rate, for example the region from 6.4 to 8.0 MeV for Fe. Using ground truth one obtains a calibration line for count rate vs Fe content, which can be used to derive Fe content for any region. This "West Coast" method, in the example given, gives results within 1σ (Table 3) about two thirds of the time.

Finally, we have used a difference method. The raw accumulated spectrum of a large lunar highland region, corrected only for gain and altitude, is subtracted from those of other regions treated similarly. The net spectrum

is positive, since Th, K, Fe, Mg and Ti are all higher in mare and KREEP regions, and O and Si about the same; only Al and Ca are lower and their contributions are small. This net spectrum is then analyzed by matrix inversion. This method gives reliable differences without making any explicit assumptions about the magnitude or shape of the continuum, or about the relative importance of continuum components. The resulting difference analyses are in satisfactory accord with those reported here, both as to the values and their errors. This constitutes in our view the strongest argument for the validity of the results reported in this paper.

In addition to these independent checks, matrix inversion analysis has, in the course of our work, been run with many modifications of procedure. The results reported are not much affected by these changes. The reader may wish to compare Table 1 in our abstract (Bielefeld et al, 1976) with Table 5 to see the differences in the Apollo 16 results produced by several small modifications in protocol.

Discussion

Regions

The regions analyzed were chosen broadly for geochemical interest. Edges correspond either to map boundaries around a given region or (especially for the equatorial, highland-rich track of Apollo 16) arbitrary meridians of longitude. In the case of mare regions labelled (L), an effort was made to stay 2° or more inside the boundary of the mare, to test the effect of contamination of data taken when the instrument was near the mare border, by photons coming from the non-mare regions in the field of view. Such effects appear to be small.

Some small geographic regions, especially Mendeleev and Hertzsprung, have a sufficient accumulation of counts because of an unusually high

fraction of prime data over these areas. Larger areas in which too little prime data is available are unfortunately more common. Thus the Grimaldi-Riccioli areas must be combined. Mare Serenitatis "inner" and "border" are regions of reported color differences. We ask the indulgence of geologists for many of the names assigned in our data tables---they are intended to be used as tags, not definitions.

Results

Discussion of the results will fall into two parts. First we will consider the data on a regional or local scale, moving generally westward down the tables. Then follow some considerations on the development of KREEP.

Mare Smythii (6B) is a mare region of intermediate chemistry; this confirms the results of Adler et al (1973) for Al and Mg. The mean compositions of the other eastern maria are broadly similar. M. Tranquillitatis shows inhomogeneity in Th and probably Ti on a scale smaller than that reported here (Reedy et al, 1975). For M. Serenitatis the Inner (5C) and Border (5D) regions represent color differences. There are no obvious chemical correlates; the color map (Frontispiece, 1973) indicates an upward trend of Th toward the west, but our lumping of the eastern and western border zones has tended to average this and possibly other differences.

In the eastern equatorial zone the series 33A, 23A, 19A, 32A shows a remarkable variety of surface topographies, from a mixed mare-highland zone, through the highlands of the Descartes landing region, to the mixed plains to the west and finally the great flat-floored crater Ptolemaeus and the rough terrain around it. Through all these changes in structure the Fe-Mg chemistry remains highland-like throughout on our scale of resolution, while a smooth rise in Th and K, like that further north, seems to require a growing admixture of KREEP.

The transition from 32A to 24A and B is sharp in Th and we believe that the true Fe in this "Fra Mauro" region is also well above that in the table, because of the neutron flux depression problem. On the western margin of Oceanus Procellarum, where KREEP is lower, there is a break in Fe between the western part of the mare and the Grimaldi-Riccioli region. The falloff in Th and K is more gradual, but still more rapid than on the east edge near Ptolemaus. On the Apollo 15 ground track the mare-highland contacts appear visually to be less abrupt.

The three radioactive "hot spots," south of Archimedes and Fra Mauro, and in the Aristarchus region, show remarkably similar Th content (all around 7-9 ppm), but distinctly different composition in other ways. Aristarchus is significantly high in Ti and Fe compared to the others. We have considered the possibility that the concordance in Th is accidental, and that the real hot spots may in one or more cases be off the ground track to the north or south, and may be still higher in Th and K. At Fra Mauro, our evaluation is constrained by the data from the Apollo 14 landing site, where Th is about 30% higher than in region 24B. There is no perceptible upward trend to the north in the orbital data. The Aristarchus peak is surrounded by lower values. At Archimedes, however, there is a downward trend to the south, and the radioactive high might well be in a few degrees north of the track, for example at the crater itself. In any case the differences in chemistry confirm that the component called KREEP is not of uniform composition everywhere.

The Orientale ejecta blanket shows no obvious north-south (outer-inner) chemical trends--only a decreasing Th concentration westward near the mare edge. On the equatorial band of the backside highlands the large craters Mendeleev and Hertzsprung (outer region) show the lowest Fe we have seen anywhere. This is unexpected, if these crater floors represent deeper exposed material.

Along the Apollo 15 track the striking backside feature around 180° longitude has been called "Van de Graaff" from its proximity to that peculiar feature. We note, however, that there is a striking correlation of the boundaries of the zone of high Fe and Th with those of the topographic low associated with the "big backside basin," (BBB) the enormous scar, 1700 km in diameter, in the southern highlands over whose edge this ground track passes at about 166°W and 162°E (Taylor, 1975).

These results show no statistically significant chemical structure within this 30° band. Recent results of K. Anderson and coworkers (priv. comm.) show that the zone of intense magnetism not only extends all across this same zone, but continues further along the southern edge of the track tens of degrees into the eastern hemisphere. Our data do not show high Th or Fe continuing into this region.

We had suggested earlier (Metzger et al, 1974) that the BBB zone might be chemically distinct from other major lunar areas. We now conclude that its chemistry is consistent with a mixture of mare and highland material, or an intermediate mare chemistry like that of M. Smythii. However, the Ti concentrations are very low.

The east-west asymmetry in the backside highland chemistry, with higher Fe and Th on the east side, persists but is somewhat less marked in these data than in earlier analyses. The differences in Mg are no longer considered statistically significant.

We return to a discussion of KREEP. The three "hot spots" represent only a small fraction of this material. The limited region so far mapped shows major concentrations extending through Oceanus Procellarum and over its boundaries, slightly to the west and very extensively to the east. The problem of its history and development is too large to be covered here. We

wish only to reiterate our view that the localization of this component (with its included K, U and Th) in the zone around 5°E to 60°W must have preceded the formation of the major maria (Metzger et al, 1973). The very large amounts of KREEP found in the Apollo 12 soil and in areas of Oceanus Procellarum seem to have been brought there by vertical mixing. At this Conference Hörz (priv. comm.) has suggested that the mean depth of the western maria is less than 1 km. whil, Gold (1976) has called attention to the absence (from long-wavelength radar data) of a clear regolith-bedrock transition in mare just as much as in highland areas. While Monte Carlo mixing models (Oberbeck et al, 1973; Langevin and Maurette, 1976; Arnold, 1975) seem to be successful in accounting for the development and properties of a regolith of a few meters depth in mare regions, they shed no light on the problems considered here.

Acknowledgements

In the period since the Sixth Conference we have been helped in the analysis of the data especially by C. S. Dyer, L. G. Evans, R. Radocinski, and R. E. Parker. We have had valuable discussions with E. Schonfeld, D. Burnett, G. P. Russ, I. Adler, L. Soderblom, and others mentioned in the text above. This work was supported in part under NASA contract NAS 7-100 at the Jet Propulsion Laboratory, California Institute of Technology, and in part under NASA contract NAS 07027. It was entirely supported by NASA.

References

Adler, I., Trombka, J. I., Schmadebeck, R., Lowman, P., Blodgett, H., Lin, L., Eller, E., Podwysocki, M., Weidner, J. R., Bickel, A. L., Lum, R. K. L., Gerard, J., Gorenstein, P., Bjorkholm, P. and Harris, B. (1973) Results of the Apollo 15 and 16 x-ray experiment. Proc. Lunar Sci. Conf. 4th, p. 2783-2791.

Arnold, J. R. (1975) Monte Carlo simulation of turnover processes in the lunar regolith. Proc. Lunar Sci. Conf. 6th, p. 2375-2395.

Berger, M. J. and Seltzer, S. (1972) Response functions for sodium iodide scintillation detectors, Nucl. Instr. and Meth. 104, p. 317.

Bielefeld, M. J., Reedy, R. C., Metzger, A. E., Trombka, J. I. and Arnold, J. R. (1976) Chemistry of the lunar equatorial zone (abstract). In Lunar Science VII, p. 58-60. The Lunar Science Institute, Houston.

Dyer, C. S., Trombka, J. I., Schmedebeck, R. L., Eller, E., Bielefeld, M. J., O'Kelley, G. D., Eldridge, J. S., Northcutt, K. J., Metzger, A. E., Reedy, R. C., Schonfeld, E., Seltzer, S. M., Arnold, J. R. and Peterson, L. E. (1975) Radioactivity observed in sodium iodide gamma-ray spectrometer returned on the Apollo 17 mission, Space Science Instr. 1, p. 279.

Foley, K. J., Clegg, A. B. and Salmon, G. L. (1962) Gamma-radiation from medium energy proton bombardment of sodium, magnesium, aluminum, silicon, phosphorus, and sulphur, Nuclear Physics 37, p. 23-44.

Frontispiece (1973), Proc. Lunar Sci. Conf. 4th.

Gold, T. (1976) The accretion of the moon. This Conference.

Harrington, T. M., Marshall, J. H., Arnold, J. R., Peterson, L. P., Trombka, J. I. and Metzger, A. E. (1974) The Apollo gamma ray spectrometer, Nucl. Instr. & Methods 118, p. 401.

Heath, R. L., Helmer, R. G., Schmittroth, L. A. and Cazier, G. A. (1965) The calculation of gamma-ray shapes for sodium iodide scintillation spectrometers, IDO-17017.

Langevin, Y. and Maurette, M. (1976) A Monte Carlo simulation of galactic cosmic ray effects in the lunar regolith. This Conference.

Metzger, A. E., Trombka, J. I., Peterson, L. E., Reedy, R. C. and Arnold, J. R. (1973) Lunar surface radioactivity: preliminary results of the Apollo 15 and Apollo 16 gamma-ray spectrometer experiments. Science 179, p.800-803.

Metzger, A. E., Trombka, J. I., Reedy, R. C. and Arnold, J. R. (1974) Element concentration from lunar orbital gamma ray measurements. Proc. Lunar Sci. Conf. 5th, p. 1067-1078.

Oberbeck, V. R., Quaide, W. L., Mahan, M. and Paulson, J. (1973) Monte Carlo calculations of lunar regolith thickness distributions. Icarus 19, p. 87-107.

Parker, R. H. (1975) Mass distribution plot of AGRS, Pasadena Observer 3, p. 2.

Reedy, R. C. and Arnold, J. R. (1972) Interaction of solar and galactic cosmic-ray particles with the moon, J. Geophys. Res. 77, p. 537-555.

Reedy, R. C., Arnold, J. R. and Trombka, J. I. (1973) Expected γ-ray emission spectra from the lunar surface as a function of chemical composition. J. Geophys. Res. 78, p. 5847-5866.

Reedy, R. C., Bielefeld, M. J., Trombka, J. I., Metzger, A. E. and Arnold, J. R. (1975) Intermare and intramare comparisons of element concentrations determined by orbital gamma ray spectroscopy. Proc. Conf. on Origins of Mare Basalts, p. 130-134, The Lunar Science Institute, Houston, Texas.

Taylor, S. R. (1975) Lunar Science: A Post-Apollo View, p. 33, Pergamon.

Trombka, J. I., Arnold, J. R., Reedy, R. C., Peterson, L. E. and Metzger, A. E. (1973) Some correlations between measurements by the Apollo gamma ray spectrometer and other lunar observations. Proc. Lunar Sci. Conf. 4th, p. 2847-2853.

Trombka, J. I., Dyer, C. S., Evans, L. G., Bielefeld, M. J., Seltzer, S. M. and Metzger, A. E. (1976a) Re-analysis of the Apollo cosmic gamma-ray spectrum in the 0.3 to 10 MeV energy region, Astrophys. Journal (in press).

Trombka, J. I., Eller, E. L., Schmedebeck, R. L., Dyer, C. S., Reedy, R. C., Barr, D. W., Gilmore, J. S., Prestwood, R. L., Bayhurst, B. P., Perry, D. G., Smith, A. E., Cordi, R. C., Pehl, R. H., Eldridge, J. S., Schonfeld, E. and Metzger, A. E. (1976b) ASTP Preliminary Science Report, TMX 58173, 7-1.

Turkevich, A. L. (1973) The average chemical composition of the lunar surface, Proc. Lunar Sci. Conf. 4th, p. 1159-1168.

Woolum, D. S., Burnett, D. S., Furst, M. and Weiss, J. R. (1975) Measurement of the lunar neutron density profile, The Moon 12, p. 231-250.

TABLE 1

Percent Composition of Average Apollo 16 Lunar Pulse Height Spectrum

	Pulse Height Energy (MeV)			
	0.4-0.8	0.8-2.0	2.0-5.0	5.0-9.0
Primary Cosmic Ray Induced Radioactivity in Detector	1.8	4.5	4.6	0.8
Secondary Neutron Induced Radioactivity in Detector	7.1	12.3	1.5	0.0
Lines Produced in Local Mass Around Detector	3.3	2.8	0.6	0.0
Electron Bremsstrahlung from Local Mass	2.8	3.5	4.0	3.4
Cosmic Gamma-Rays	4.0	3.0	2.2	1.4
Induced and Natural Radioactivity in Spacecraft	5.1	4.6	5.4	7.1
Multiple Scatter from Moon Due to Variations in Th, U & K	4.8	1.8	0.1	0.0
Multiple Scatter from Moon at Lowest Concentration of Th, U & K	56.1	58.0	71.3	73.0
Discrete Lunar Lines	15.0	9.5	10.2	14.1
Total (%)	100.0	100.0	100.0	100.0
Total (counts/second)	55.2	45.8	25.3	8.6

TABLE 2

Ground Truth: Nominal Compositions and Normalization Factors

	E. Mare	W. Mare	KREEP	High-land	BBB	Calculated Apollo 15 mean	Calculated Apollo 16 mean	Turkevich whole moon	Apollo 15 Ground Truth Norm. Factor	Apollo 16 Ground Truth Norm. Factor
Fe(%)	12.1	12.5	8.1	4.0	7.7	6.5	6.1	5.8	0.85±.05	1.04±.07
Mg(%)	4.8	6.2	5.6	3.3	3.8	4.0	4.0	4.7	0.53±.03	0.71±.05
Ti(%)	4.5	1.7	1.0	0.3	0.1	0.9	0.8	0.8	(1.1)	(1.2)
Ca(%)	8.5	7.3	7.8	11.3	(9.9)	10.2	10.3	10.7		
Al(%)	7.2	6.7	9.3	14.5	(10.8)	12.1	12.5	11.7	0.65±.07	0.56±.08
Si(%)	19.6	21.5	22.3	21.1	22	21.1	21.1	21.3		
O(%)	40.8	42.0	44.0	45.2	44	44.1	44.2	44.0		
K(%)	0.10	(0.20)	0.44	(0.08)	0.16	0.13	0.11			
Th (ppm)	1.92	(6.0)	11.6	0.7	2.3	2.6	2.0			

TABLE 3

Error Estimates (σ) for Data in Tables 4 and 5

(In the formulas c is the concentration in ppm)

Element	Time-Independent	Counting-Time-Dependent Coefficient of $(t/2000\ sec)^{-1/2}$
Th	$((0.15)^2 + (0.1c)^2)^{1/2}$ ppm	Small
K	$((130)^2 + (0.1c)^2)^{1/2}$ ppm	100 ppm
Fe	0.8% (but see text for KREEP-rich regions)	0.6%
Mg	0.6%	1.5%

TABLE 4

Chemistry of Regions (>2000 sec)

Apollo 15

Region	Name	Longitude (Area)	Time	Th ppm	K ppm	Fe %	Mg %
15A	High E. Front	55-90°E	7600s	1.1	900	7.4	5.6
15C	High E. Front	63-78°E	4800	1.3	650	6.9	6.1
3A*	M. Fecund.	44-61°E	2100	1.9	970	10.6	5.2
16C*	Mixed Zone	30-62°E	4000	1.7	1000	9.3	4.1
7C*	M. Tranq. East	30-45°E	3200	1.6	1100	9.1	5.8
7A*	M. Tranq.-Total	18-45°E	4600	1.8	1100	9.4	4.9
7F*	M. Tranq.-Ti-low	18-45°E	3400	1.8	1200	10.1	4.5
7B*	M. Tranq.-(L)	22-42°E	3000	1.9	940	9.1	5.6
5A*	M. Seren:Total	9-29°E	4000	1.9	1300	11.7	4.8
5D*	M. Seren:Border	9-29°E	2000	2.2	1400	11.6	5.2
5C*	M. Seren:Inner	12-26°E	2000	1.5	1300	11.9	4.6
5B*	M. Seren:(L)	11-26°E	2600	1.7	1200	12.6	4.7
21A	Archimedes	2°E-8°W	2800	7.1	3400	5.5	3.6
4C	M. Imbrium:East	9-20°W	3100	5.7	2300	10.0	4.1
4A	M. Imbrium:Total	9-33°W	6600	5.4	1900	10.7	4.9
4B	M. Imbrium:West	20-33°W	3500	5.1	1500	11.3	5.9
22A	Aristarchus	42-54°W	3400	6.5	2600	9.1	6.4
9A	Oc. Proc. North	50-78°W	5700	3.7	1800	10.2	2.7
10B*	Highland Boundary	65-86°W	2900	1.7	930	7.1	4.1
11A	Highland W. Limb	86-120°W	7700	0.65	670	4.5	3.8
28A*	Hertzsprung South	120-138°W	2300	0.65	750	5.2	3.4

TABLE 4 (continued)

Chemistry of Regions (>2000 sec)

Apollo 15

Region	Name	Longitude (Area)	Time	Th ppm	K ppm	Fe %	Mg %
12C	Highland W. Farside	120-140°W	4000	0.83	530	6.0	5.0
12A	Highland W. Farside	120-166°W	11700	0.88	620	5.4	4.6
12B	Highland W. Farside	140-166°W	7800	0.91	660	4.8	4.4
35D	BBB:West	166-178°W	3100	2.2	1500	8.4	5.0
35A*	BBB:Total	166°W-162°E	9500	2.5	1500	7.7	4.8
35C	BBB:Center	178°W-170°E	3800	2.8	1800	6.0	4.3
35B	BBB:(L)	168-177°E	2800	3.1	1700	5.6	5.6
35E	BBB:East	162-170°E	2500	2.4	860	8.4	5.4
13C*	Highland E. Farside	120-143°E	5800	0.72	640	6.2	3.9
14E	Highland E. Limb	90-120°E	7200	0.61	430	5.6	3.5
36A	Whole Moon	All	104000	2.3	1200	7.7	4.5

Footnotes:

*Regions containing less than the whole body of data for the given longitudes. Those identified as (L) have borders about 2° inside the corresponding total region.

3A - Within boundaries of M. Fecund---reaches 6°N around 50°E.

16C - Highlands North of 3A.

7 - Mare Tranquillitatis --- all within mare borders, 7C - East of 30°E, X-ray data suggest higher Al. 7A - Total. 7F - Total minus a region 0 - 10°N and 24-40°E considered high in Ti from energy band analysis.

TABLE 4 (continued)

Footnotes:

5 - Mare Serenitatis. 5A - Total. 5C - a shield-shaped inner-region from 12-26°E, of higher albedo than 5D. 5D - Total minus 5C; two vertical strips of lower albedo converging at the bottom.

9A - Bounded to southwest by the highland margin.

10B - Bounded to northeast by 9A.

28A - Southern boundary 9°S at 130°W, rising to 3°S at the east and west ends.

35A, D - south of 20°S

13C - excludes Tsiolkovsky

TABLE 5

Chemistry of Regions (>2000 sec)

Apollo 16

Region	Name	Longitude (Area)	Time	Th ppm	K ppm	Fe %	Mg %
6B	M. Smythii	80-93°E	2000	1.4	870	8.6	3.9
15D	High E. Front	63-78°E	6200	1.2	920	6.7	4.1
15B*	High E. Front	55-81°E	9300	1.2	830	7.6	4.4
3B*	M. Fecund.	42-61°E	6100	1.5	1000	10.7	4.6
16B	Mixed Zone	30-42°E	3900	1.5	1000	7.7	5.3
33A	Theophilus Reg.	22-30°E	3100	1.7	880	5.3	3.5
23A	Descartes	12-22°E	4300	1.8	1200	5.5	5.3
17A	High. Central	5-26°E	8900	2.2	1100	4.9	5.5
19A	Andel	6-12°E	2500	2.8	1400	3.4	5.5
32A	Ptolemaus	1°E-4°W	2000	4.9	2600	4.6	6.8
24B	Parry-Bonpland	8-14°W	2200	9.0	3100	4.9	6.9
24A	Fra Mauro Reg.	5-20°W	5600	8.2	3100	5.3	7.0
1A	M. Cognitum	20-23°W	2800	6.7	2600	8.8	5.3
9B	Oc. Proc. South	30-58°W	11300	4.3	1900	10.4	6.8
9D	High. Border	58-65°W	3100	2.6	1600	4.7	5.4
10A	Grimaldi-Ricc.	58-86°W	12000	1.7	930	4.1	2.1
31A*	Orientale Rings	76-110°W	4100	0.60	640	5.0	1.9
11B	High.W.Limb	78-120°W	13300	0.54	660	3.8	2.9
28B*	Hertzsprung	120-138°W	5200	0.44	650	2.7	2.2
12F	High.W.Farside	120-150°W	10700	0.31	690	3.9	3.2
12D	High.W.Farside	120-180°W	23000	0.33	630	4.5	2.7

TABLE 5 (continued)
Chemistry of Regions (<2000 sec)
Apollo 16

Region	Name	Longitude (Area)	Time	ppm	ppm	Fe %	Mg %
29A	Korelev Ejecta	145-170°W	9900	0.14	770	5.3	2.5
12E	High.W. Farside	150-180°W	12400	0.32	580	4.8	2.3
13E	High.E.Farside	150-180°E	11600	0.48	690	5.5	3.6
13D	High.E.Farside	120-180°E	18800	0.56	600	5.4	3.5
30A*	Mendeleev	136-147°E	2700	0.26	850	2.0	3.6
13F	High.E.Farside	120-150°E	7200	0.66	460	5.1	3.6
18B	Al-Khwarizmi	103-122°E	3200	0.39	450	5.6	2.7
14B	High.E.Limb	94-120°E	4500	0.38	650	5.5	2.0
36B	Whole Moon	All	127000	1.9	1100	6.3	3.8

Footnotes:

*Regions containing less than the whole body of data for the given longitudes 15B: Omits 61°-59°E and some other spots. 3B: Omits data over Langrenus B and nearby craters. 31A: Omits data north of 2°S. 28B: Omits data outside the outer Hertzsprung boundary. 30A: Omits data outside Mendeleev.

Figure Captions

Figure 1. Total gamma ray spectrum (Apollo 16) showing the components of background into which it has been decomposed, and the net spectrum due to lines in the lunar surface. The energy scale is 19.3 KeV/channel.

Figure 2. The net spectrum due to lines in the lunar surface (see Figure 1), showing the individual elemental components (O, Si, Fe, Ti, Mg, K, (Th + U)) as determined by matrix inversion. The positron line is at 0.511 MeV; the ^{203}Hg calibration line is at 0.279 MeV. The top curve represents the total synthesized spectrum.

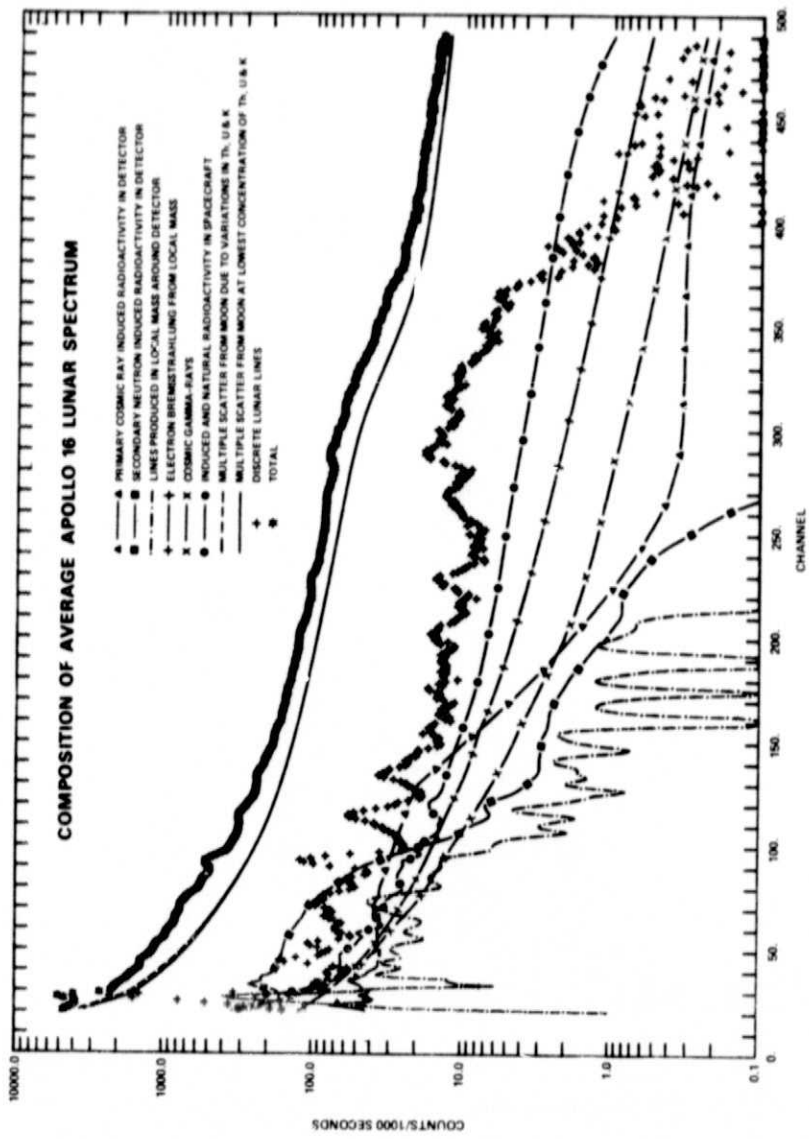

Figure 1

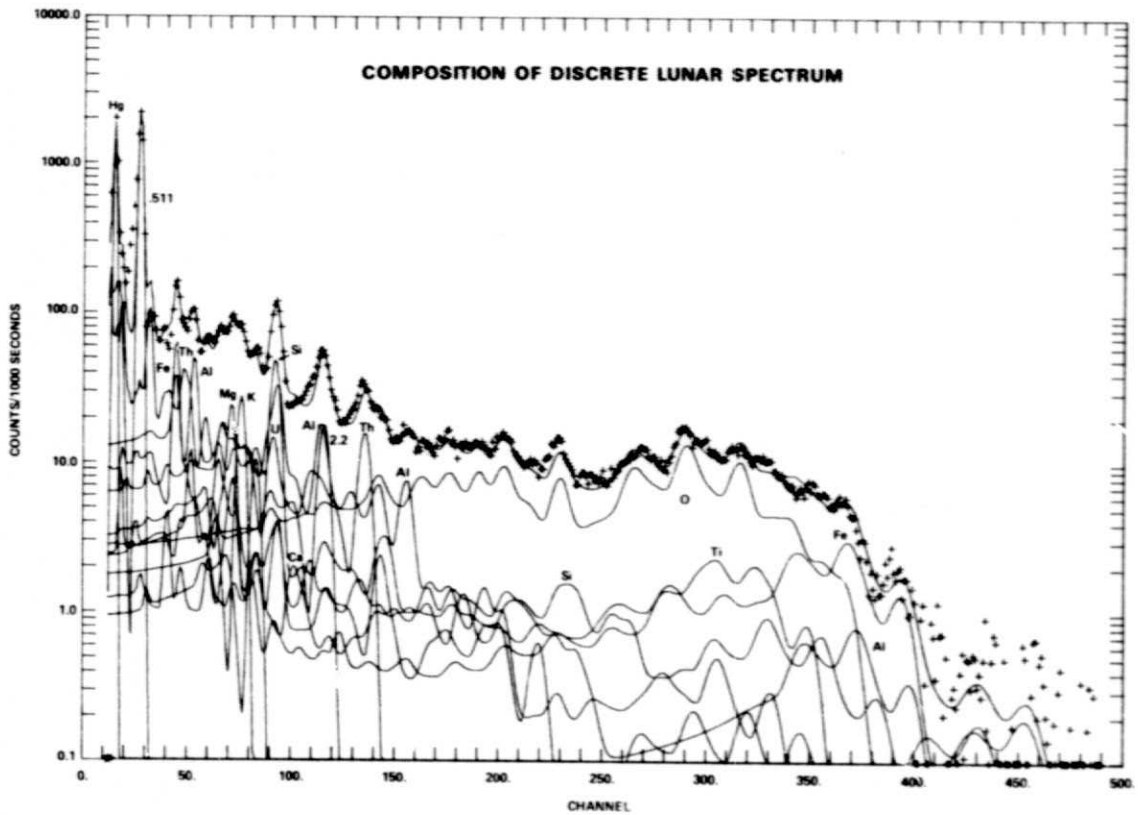
COMPOSITION OF DISCRETE LUNAR SPECTRUM
COUNTS/1000 SECONDS
CHANNEL
10000.0
1000.0
100.0
10.0
1.0
0.1
0.
50.
100.
150.
200.
250.
300.
350.
400.
450.
500.
Hg
.511
Fe
Th
Al
Mg
K
Si
Al
2.2
Th
Al
O
Si
Ti
Fe
Al
Ca

Figure 2